OFEL
524

Detection of surface laid and buried mines with IR and CCD cameras, an evaluation based on measurements

Yvonne H.L. Janssen, Arie N. de Jong, Hans Winkel and Frank J.M. van Putten

TNO Netherlands Organisation for Applied Scientific Research, Physics and Electronics Laboratory
P.O. Box 96864, 2509 JG The Hague. The Netherlands
E-mail: Y.H.L.Janssen@fel.tno.nl

ABSTRACT

We analysed a time series of high resolution 8-13.4 μm scanner images of a sandbox with buried (3-10 cm depth) and unburied, metal and plastic AP and AT mines, surrogates and other targets. With a high resolution DUDA scanner operating in 8-13.4 μm all the surface laid targets were visible during the whole diurnal cycle. The buried targets were only visible during sunrise and sunset. The emissivity of the targets and sand could not be derived from the measured apparent temperatures and contact temperatures.

Keywords: mine detection. landmine, thermal infrared sensors, temporal behaviour

1. INTRODUCTION

Real time detection of all kinds of landmines in different environments, weather conditions, seasons and at different times of day can be done with a system that combines detection in several spectral bands and using different detection principles. Systems operating in various infrared spectral bands are strong candidates because of all weather and day and night capability, speed (real time) and mature technology status.
Recent studies have demonstrated the feasibility to detect both buried and unburied metal and plastic mines[1-7] with infrared imagers. In the Mideast (Desert Storm) landmines were sighted through tank infrared weapons sights[1]. Experimental airborne infrared detection systems showed that even buried AT (anti tank) mines could be detected with dual-band infrared imagers[5-7].
The purpose of this paper is twofold. The first is to evaluate if high resolution thermal viewing devices are able to detect plastic as well as metal mines, both AT and AP (anti personnel), buried and surface laid. The second is to record time series with available VIS (visual), NIR (near infrared) and TIR (thermal infrared) viewing devices. Data of these devices are compared with other sensors and are used to model thermal contrasts of landmines in different environments, at different times of day and various climates. To meet these objectives, images of a surrogate minefield obtained during a complete diurnal cycle were analysed with respect to the mine-background contrast.

2. TEST CONDITIONS

2.1 Location

Part of the dunes located near the TNO-FEL building at The Hague in The Netherlands. were used as test site (52.11 ° N, 4.32° E). The test site is surrounded by open terrain, sparsely covered with grass, moss, scrub and small trees. The testbed was a layer of humid and dry white sand, not covered by vegetation.

2.2 Types of mines

The targets that were used during the experiment can be devided into five categories and are shown in figure 1.

- metal AT mines, such as, DM31
- plastic AT mines, such as, L128, TMA2, TMA3, TMA4 and TMA5
- surrogate AT mines, such as, AT1, AT2, AT3 and AT4
- AP mines, such as, AP22 and butterfly
- potential false targets such as cans, glass, rocks, tiles and dummy holes.

As can be seen in figures 1 and 4 the last two rows of mines are surface laid. the front two rows are buried. Depth of burial varies from 3 to 10 centimetres. The size of the AT mines varies from 10 to 30 cm, except for the bar mine, the size of the AP mines

 0-8194-2146-4/96/$6.00

TNO
18852

mines varies from 1.5 to 6.0 cm. The filler material of the plastic AT mines is made of a hardened castor oil. The surrogate AT mines, i.e., AT1 - AT4 are made of massive aluminium, foam filled and hollow aluminium and massive plastic respectively.

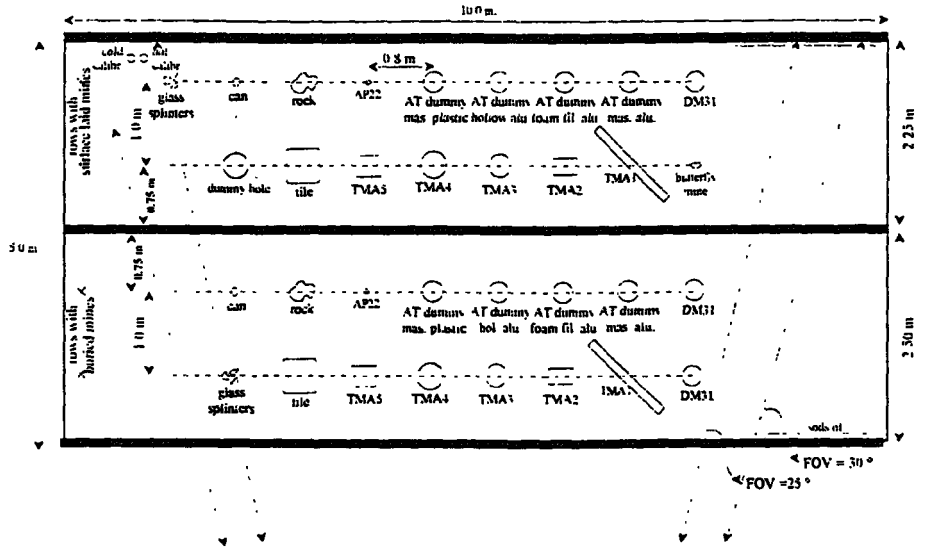

Figure 1: Set up of surrogate minefield.

2.3 Mine Field installation

The minefield was installed in an open flat area of 5 m x 10 m which was cleared of all vegetation. The remaining sand was compact, moist but not wet at the time of placement of the mines. The mines were placed by hand without entering the test area, using a wooden bar in the middle of the minefield. A 1.5 m wide stroke of grass was placed on the right hand side of the minefield. After all the mines were laid out the whole area was moisturised with a rain installation to make sure most variations in roughness and soil moisture were cleared. During the two-day interval between installation and first viewing, the weather was hot and dry. When the test began on August 21 still differences in moist between the left and right part of the test area were noticeable. This lasted till the last day of the experiments, August 25. Digging scars and thermocouple wires were invisible during the whole week of experiments except for the wooden bar that was used for installation of the minefield.

2.4 Recording systems

Images of the surrogate minefield were recorded with the at TNO-FEL designed DUDA system, a system combining TIR scanning imagers operating in 3.7-5.5 and 8-13.4 μm. Other recording systems are a focal plane array (FPA) of InSb operating in 2.27 - 4.67 μm, a InGaAs FPA operating in 0.9-1.7 μm and another at TNO-FEL designed system called MSCCD, a system combining three CCD cameras filtered in narrow spectral bands around 550, 670 and 800 nm. During the experiment also images were obtained with an imaging 94 GHz radiometer[8]. In this article only the results of the 8.0-13.4 μm DUDA scanning imager will be discussed. Characteristics of the camera systems are given in Table 2.

System	wavelength band	NETD [°K]	IFOV [mrad]	FOV	bits
DUDA, scanning imager	3.7 - 5.5 μm 8.0-13.4 μm	.02	1.0 x 1.0	30 x 7.5/15 ° ≈ 4096 x 1024 pixels	12
InSb FPA, type IRC160	2.27 - 4.67 μm	.02	1.0 x 1.0	9.1 x 6.8 ° ≈ 160 x 120 pixels	12
InGaAs FPA	0.9 - 1.7 μm	-	0.44 x 0.44	3.26 x 3.26 ° ≈ 128 x 128 pixels	12
MSCCD, 3 boresighted CCD cameras	550 nm 670 nm 800 nm	- - -	0.27 x 0.27	4.6 x 3.5 ° ≈ 512 x 512 pixels	12

Table 2: Characteristics of VIS, NIR and TIR camera systems.

A weather station measured the local air temperature, wind direction and speed, relative humidity, global irradiance, atmospheric pressure and rain rate (the rain sensor turned out to be defect). Because the sky temperature can be an important factor, cloud cover estimates of a nearby meteorological station were used.
The temperatures of the mines and surrogates and the sand backgrounds at the surface and depths of 3, 13 and 13 cm were measured with thermocouples. Also the temperatures of the hot and cold black body were measured.

2.5 Set-up

The camera systems were placed on a platform. The horizontal distance between the radiometer and the surrogate minefield was about 15 meters. The centre of the camera systems on the platform was 5.0 m above groundlevel. Figures 3 and 4 show the set-up of the surrogate minefield and the platform with the camera systems. The mines were viewed at elevation angles varying from 16.0° to 21.8 °.

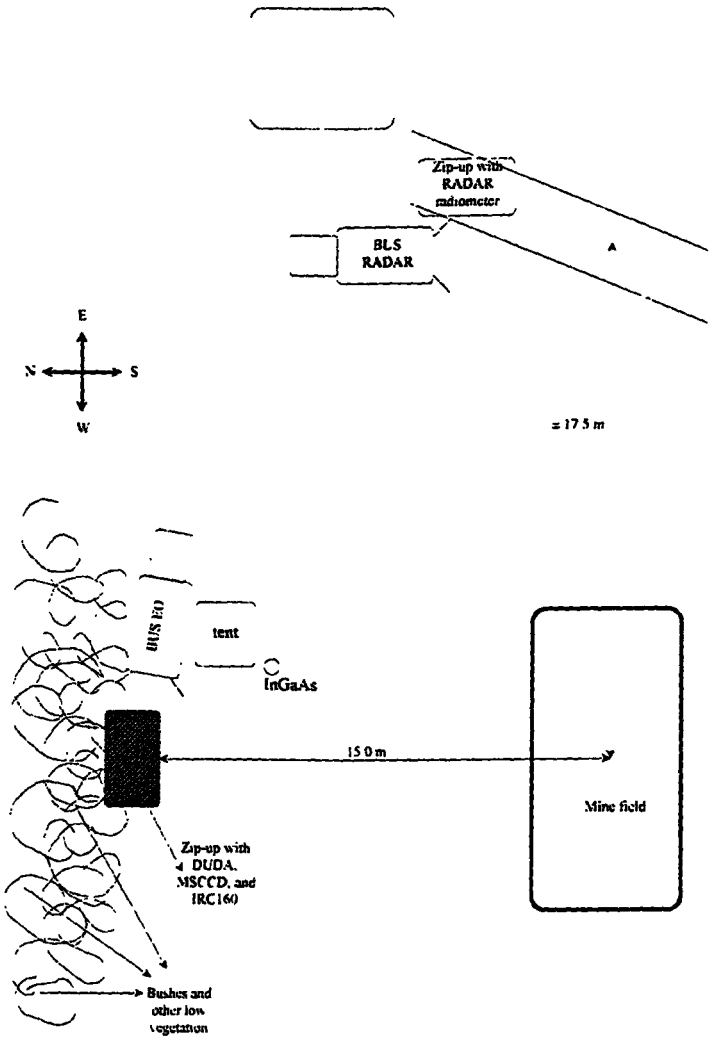

Figure 3: Set up of surrogate minefield and platform with TIR and VIS camera systems.

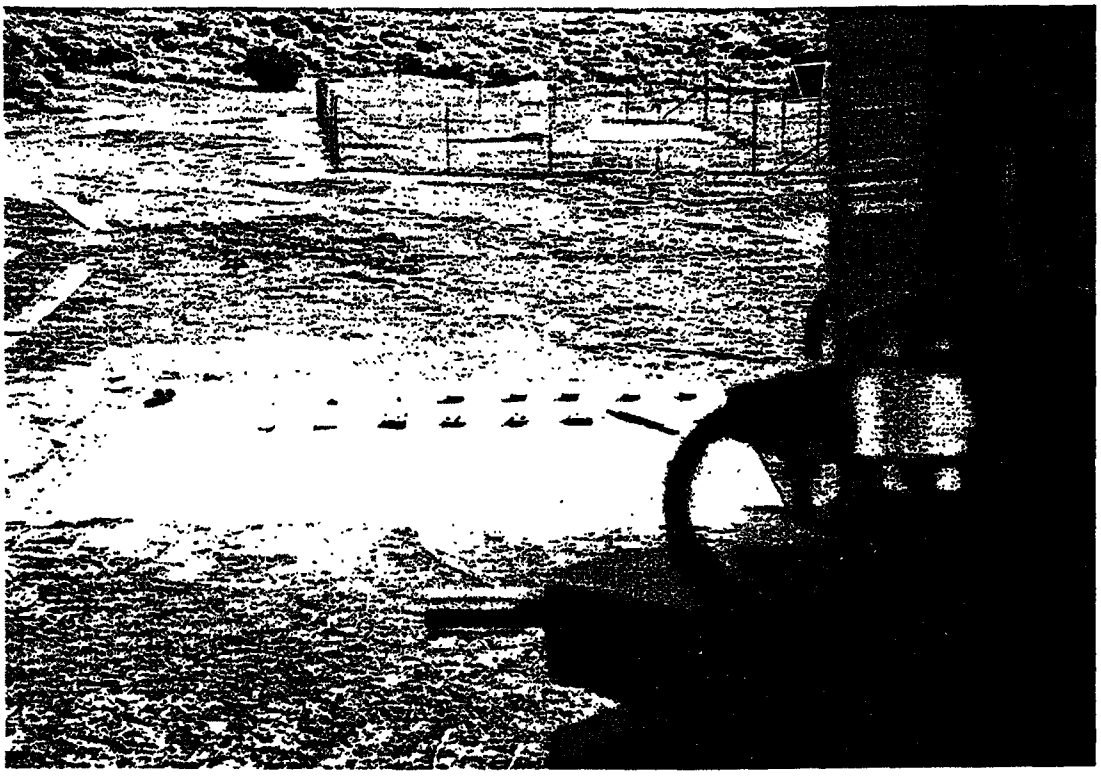

Figure 4: Set up of surrogate minefield seen from platform with camera systems.

2.6 Thermal infrared calibration

The internal calibration routine of the DUDA imager includes the transmission losses of the optics, the responsivity of the detector and the correction for the front window. This results in coefficients that will fit the voltage measured from the sensor for the internal black body sources to expected voltages for the sources. The accuracy of the at TNO-FEL designed DUDA system[9] is within 0.2 °C and based on field tests and calibration with an objective MRTD measurement[10].
The external calibration of the thermal infrared camera systems is based on two black body reference sources, one hot and one cold, as can be seen in the top left corner of Figure 1 and 5. The cold calibration source is always 2.0 °C higher then the ambient temperature. The hot calibration source is always 6.0 °C higher then the cold one. By measuring the black body (apparent) temperature of these reference sources and correlating them with the corresponding pixel intensity values, each pixel in the image can be calibrated. Through this procedure a temperature (°C) or irradiance (W/m^2) value can be assigned to all pixels.

2.7 Recording procedures

Between 15:00 on August 22 and 11:00 on August 24 1995, images were recorded every half hour with the systems as mentioned in Table 2, except for the InGaAs FPA. Images were not recorded simultaneously but one at a time. First the DUDA images were recorded, then the IRC160 images and finally the MSCCD and InGaAS images. Consequently there is a time shift of 3-5 minutes between the DUDA and MSCCD recordings. Images of the InGaAs FPA were only recorded on occasionally.
Because the FOV of the DUDA scanner is big enough to contain the entire minefield, it was not moved during the test. The maximum shift between DUDA images is 2 pixels due to fluctuating windspeed and movement of the tri-pod of the MSCCD and IRC160.
The FOV of the MSCCD and IRC160 systems was not big enough to view the total minefield. For these systems the minefield needed to be recorded in three steps. Therefore the systems were mounted together on a tri-pod. The movement in elevation and azimuth was controlled by a computer resulting in an accuracy in step size of 0.5 mrad and 1.5 mrad respectively.
The meteorological data were measured every 5.0 seconds and stored as averaged values over a period of five minutes. Data of the thermocouples were recorded every 5 minutes.

3. RESULTS

In this paper we will focus on the thermocouple and DUDA (8-13.4 μm) data recorded on August 23, 1995. Data recorded on August 22 and August 24 resemble the data of August 23.

3.1 TIR data

3.1.1 Thermal imagery collected with 8-13.4 μm channel of DUDA

A sample of the thermal imagery collected with the 8-13.4 μm channel of the DUDA is shown in figures 5a and 5b. The individual images of this time series have been scaled for presentation purposes so that the individual targets can be seen more clearly. Almost all collected DUDA imagery is of high quality and can be used for further analysis.
Because of a warping of the image (for representation in this paper) to a lower resolution and a decreased contrast (32 grey levels instead of the available 4096) not all of the results presented in figures 5a and 5b are clearly visible.

A qualitative inspection of the presented images revealed that:

1. All the surface laid mines are good detectable against the sand background during day and night. This holds for metal and plastic AT and AP mines. Only for a short period of day (several minutes) the contrast between mines and background was so low that they were invisible.
2. All the surface laid potential false targets (can, rock, dummy hole, tile and glass pieces) were visible during the whole period of 24 hours.
3. Several of the buried mines were detectable during two periods of a day, namely around sunrise (08:00) and sunset (19:00). Only the buried mines that were covered with dry sand (right part of the image) were visible.
4. During night time (before 07:00 and after 21:00) the contrast between most of the mines and the sand is positive. During daytime the contrast between the mines and the sand is positive or negative depending on the side of the mine.
5. The contrast between the top and the side of the surface laid mine is often of the same order as the contrast against the sand.

3.1.2 Apparent temperature contrast of targets against sand

A more quantitative analysis of these data can be given by means of apparent temperature contrast between a mine and its backgrounds. The apparent temperature contrast is derived from the grey level of the image pixels as described in section 2.6. The average apparent temperature contrasts as presented in Figure 6 is based on an average contrast over the side of the mine and an average contrast over a part of the sand near the mine.

For all targets, as well surrogate mines and potential false targets, the trend is a decrease in average absolute apparent temperature contrast between 07:00 and 13:00, being a contrast change from positive to negative. Between 14:00 and 18:00 this trend is followed by an increase in absolute average apparent temperature contrast. After this period, during night time, the average apparent temperature contrast between the mines and the sand background is rather stable with several degrees Celcius.
Before 07:00 and after 18:00 the contrast in average apparent temperature for all mines between the side of the mine and the sand is bigger then between the top of the mine and the sand. Between 09:00 and 16:00 this phenomenon is reversed for the plastic (solid or cased) mines TMA2, TMA3, TMA4, TMA5 and AT4. During that same period of day the metal (solid and cased) mines, AT1, AT2 and AT3 show the same phenomenon as during night time, i.e., opposite behaviour to the plastic mines.
For all mines and most of the potential false targets there is a discontinuity, i.e. not a smooth change, present in average apparent contrast around 07:00. The metal mines AT1, AT2 and AT3 and the metal can show the largest variations (-5 °C -> +5 °C)in averaged apparent contrast during the period of 24 hours. During this period the solid plastic mine AT3 shows the smallest variation in average apparent contrast. Most of the plastic cased mines show an increase, i.e. lower absolute contrast value around 13:00.
The absolute average apparent contrast between the potential false targets and the sand varies from small values, i.e. 1 °C up to bigger values, i.e. 7 °C, respectively for glass, tile, rock, hole and can.

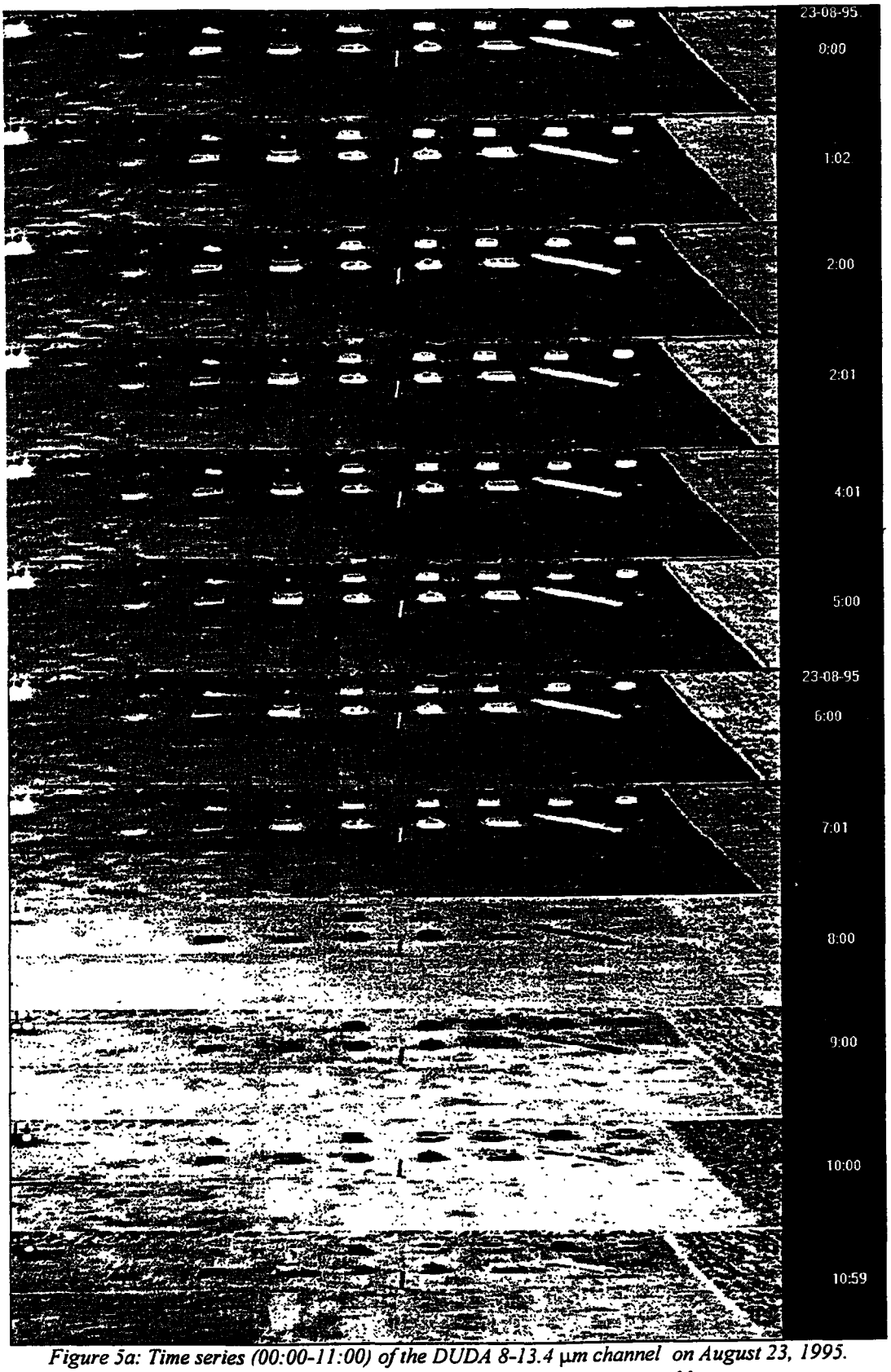

Figure 5a: Time series (00:00-11:00) of the DUDA 8-13.4 μm channel on August 23, 1995. Only parts of the 4096 x 1024 pixels images are presented here.

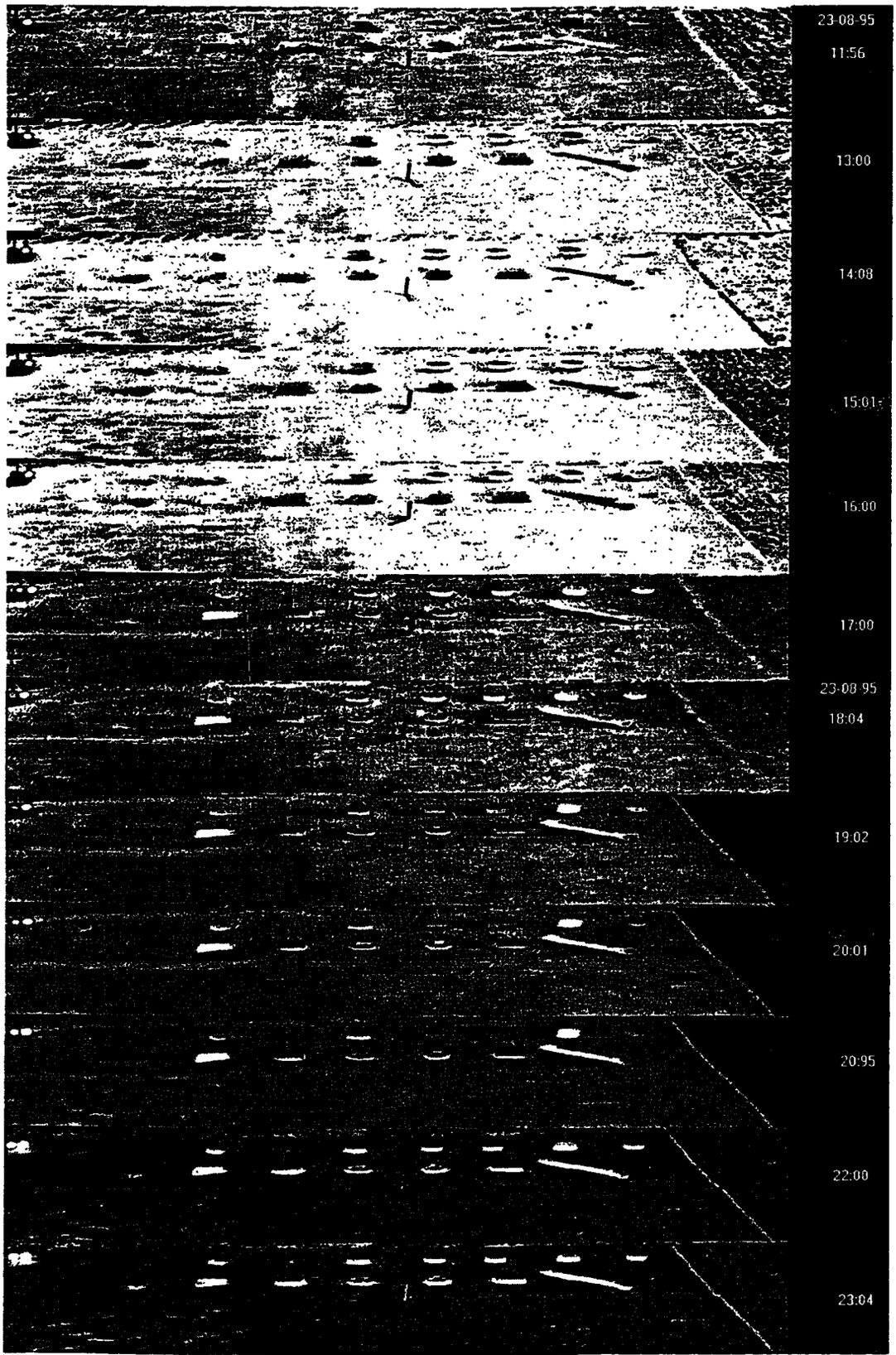

Figure 5b: Time series (11:56-23:04) of the DUDA 8-13.4 μm channel on August 23, 1995. Only parts of the 4096 x 1024 pixels images are presented here.

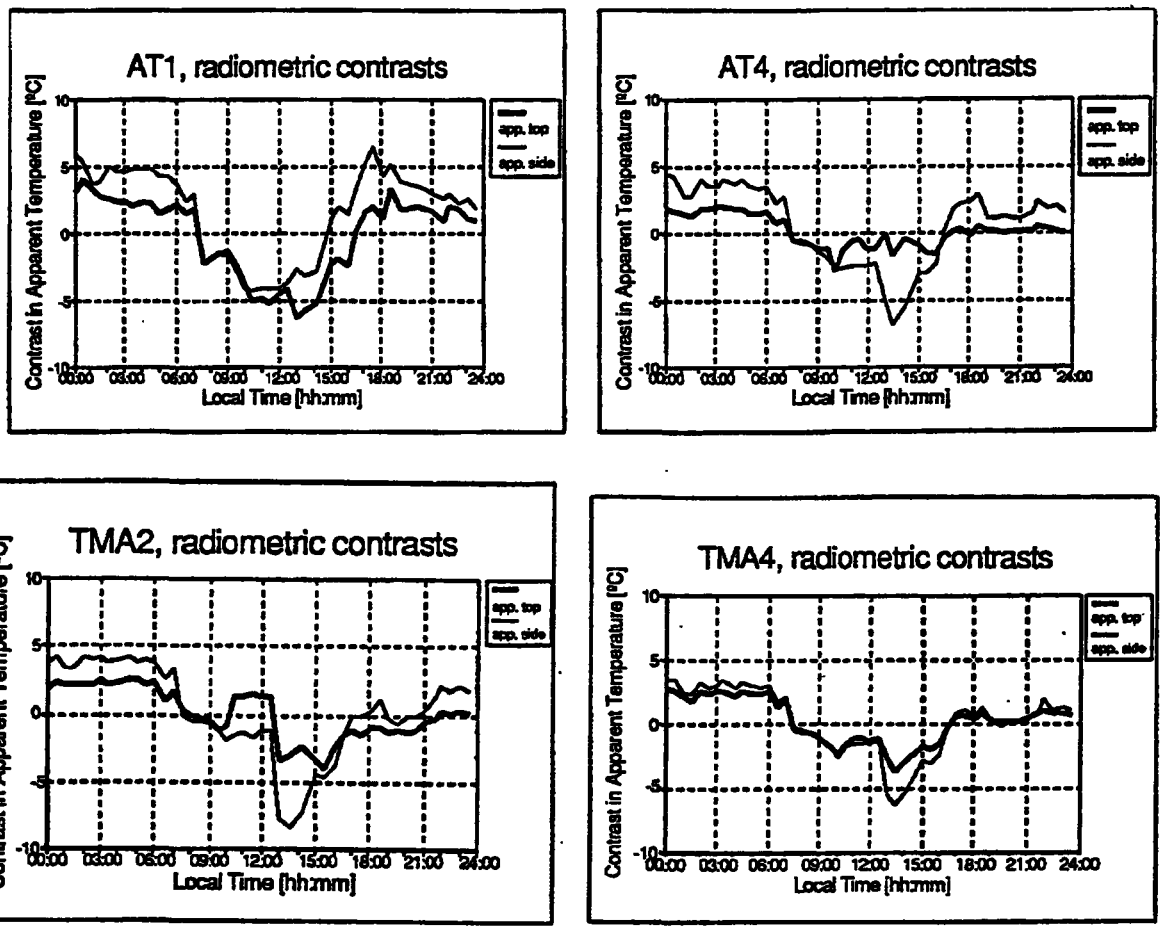

Figure 6: Examples of apparent DUDA 8-13.4 μm temperature contrasts. Time period: Aug. 23 00:00 to 24:00 h. local time. App. top corresponds with the average apparent temperature of the top side of a mine. App. side corresponds with the average apparent temperature of the side of a mine.

.2 Weather data

'igure 7 shows the for this paper relevant weather data of August 23, 1995. The whole day represented a rather hot summer day or the Dutch dunes. The relative humidity was high and there was almost no cloud cover until 16:00.

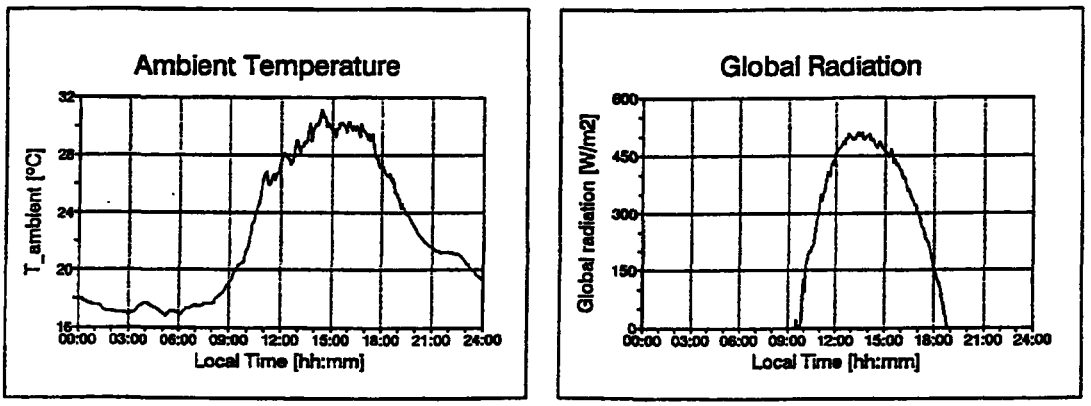

Figure 7: Ambient temperature and global radiation of August 23, 1995.

3.3 Thermocouple data

The temperatures of both the surface laid and buried targets and sand backgrounds were measured with thermocouples. In the discussion in section 4.3 we focus on the apparent temperature contrast of the targets against the sand.
The apparent contrast between a mine and the background depends on, among other factors, the absolute temperature difference between a mine and the background. In figure 8 therefore the mine temperatures minus the sand surface temperature are shown.

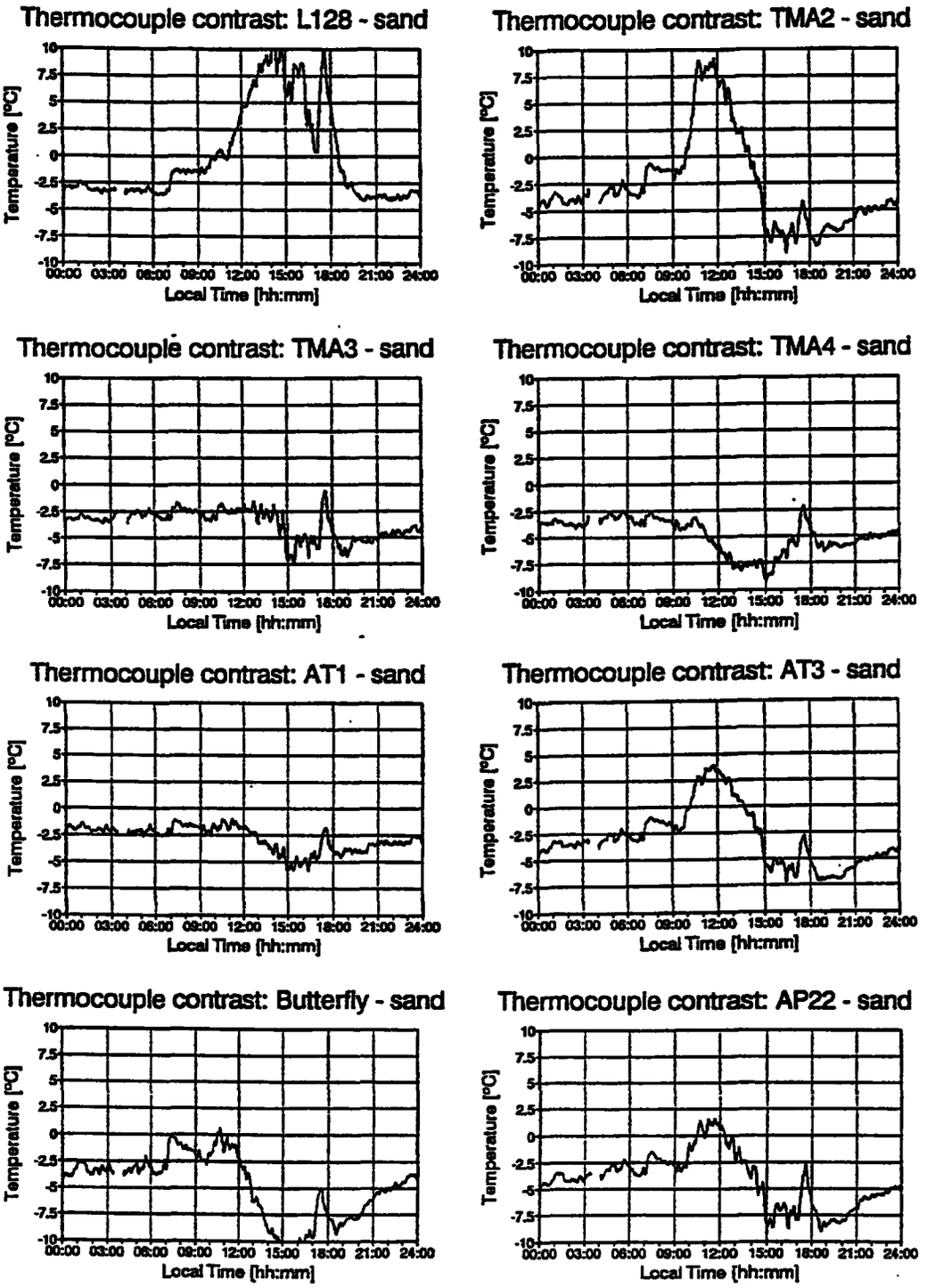

Figure 8: Contact temperature contrasts. Time period: 00:00 to 24:00 of August 23, 1995.

The average trend is a contrast increase between 09:00 and 12:00, a decrease between 12:00 and 18:00 and a moderate increase from 18:00 to 09:00. Before 09:00 and after 15:00 the contact temperature contrast is negative and constant. For a period of time between 09:00 and 15:00 the contrast of almost all the mines becomes positive. The positive peak in contrast is for almost all mines, except for the TMA3 and TMA4 , around none. The negative peak or drop in contact temperature contrast occurs for all mines around 16:00. The L128, TMA2 and TMA3 show the biggest variation (12.5 °C) in temperature contrast, while the AT4, TMA3 and TMA4 show the smallest variation (5 °C). The AP mines, AP22 and butterfly, and the AT1 have during almost the hole period of day a negative temperature contrast.

4. RESULTS, DATA ANALYSIS

4.1 Contact temperature contrasts

Depending on the variation in contact temperature contrast (cf. section 3.3), the mines can be devided into three classes:

1. The small AP mines and the solid aluminium AT1 mine. These show a negative temperature contrast with the sand during the whole day. Due to their size or homogeneous material properties these mines absorb the solar irradiance at the same rate as the sand does. At 12:00 the temperature of the mines is close to ambient temperature. After 12:00 thermocouple temperature contrast between the mines and the sand becomes more negative because the mines have a good heat exchange with the surroundings. E.g. the AT1 mine has a much higher heat conductivity ($\lambda_{aluminium} \approx 237\ Wm^{-1}K^{-1}$) > $\lambda_{dry\ sand} \approx 1\ W\ m^{-1}K^{-1}$)[11] and therefore adapts much better to the ambient temperatures. After 15:00 the temperature contrast starts decreasing because both the mines and sand have reached their maximum temperatures because is at maximum elevation.
2. The solid plastic AT4 and the plastic cased TMA3 and TMA4 mines. These targets have almost a constant negative temperature contrast of several degrees in time. This constant temperature gap between the target and sand is a result of identical netto heat exchange processes of both.
3. Before 09:00 and after 18:00 the other mines have a rather constant negative temperature contrast. These contrasts are constant because during this period of a day the direct heating effect by solar energy can almost be neglected and a state of equilibrium is reached. At 09:00 direct solar energy starts heating up the mines. Because the heat capacity of these mines is higher ($C_{polyetheen} \approx 1.4\text{-}2.2 \times (10^3\ Jkg^{-1}K^{-1})) > C_{dry\ sand} \approx 0.8 \times (10^3\ Jkg^{-1}K^{-1})$)[11] then of the surrounding sand, these mines absorb more of the solar energy then the sand. Around 12:00 the mines have almost the same temperature as ambient. From that moment on the temperature contrast between the mines and sand starts decreasing until the moment that the heating effect of the sun can be neglected.

4.2 DUDA radiometric apparent temperature contrasts

The detected infrared radiation from an object depends on contact temperature and emissivity ε. Emissivity ($0 < \varepsilon < 1$) is a surface characteristic that indicates how well an object approximates a blackbody, or a perfect radiator. Emissivity values near one ($\varepsilon \approx 1$) indicate good radiators, whereas emissivities near zero ($\varepsilon \approx 0$) indicate to mirror like objects. A calibrated thermal image (section 2.6) gives the "apparent" temperature of an object because the emissivity of an object is not known, so the calibration program treats al the objects as though they are blackbodies.

Based on the variation in average apparent temperature contrast (cf. section 3.1.2) the mines and minelike targets can be devided into two classes:

- Metal and metal cased mines, i.e. AT1, AT2 and AT3. During the whole 24 hours the top of the metal mines have a lower apparent contrast against sand. Since the heat capacity and heat conductivity are the same for the side and top of the mine, this has to be a result of the emissivity of the mine (ε_{mine}) that has a lower value then 1 and the difference in slope. The emissivity of the metal mines with army green paint is approximately 0.9. The apparent temperature of the top of the mine is also influenced by reflected cold sky. The side of the mine reflects a part from the cold sky and a part of the surrounding sand. This results in a higher apparent temperature of the side then of the top.
- Plastic and plastic cased mines, i.e. , AT4, L128, TMA2-TMA5. Between 09:00 and 16:00 the top of the plastic mines have compared to the side a higher apparent temperature contrast against the sand. This is opposite to the apparent temperature contrasts of the metal mines during the same period of day. This is probably caused by a difference in emissivity between the plastic and metal. The emissivity of non painted plastic mines is higher then of non painted metal.

In general all targets show a similar thermal behaviour, i.e., a maximum in positive apparent temperature contrast between 00:00 and 03:00 and a maximum in negative apparent temperature contrast around 14:00.

4.3 Comparison thermocouple and average apparent temperature contrasts

If all the objects in the images were blackbodies then the apparent temperature would equal the contact temperature. In reality, since most objects are not black bodies, their contact temperature differs from the apparent temperature. Therefore the contact temperature contrast and the apparent temperature contrast between the mines and sand is different.
The apparent temperature contrast can be written as:

$$T_{mine,app} - T_{sand,app} = (\varepsilon_{mine}.T_{mine,cont} - \varepsilon_{sand}.T_{sand,\ cont}) + ((1-\varepsilon_{mine}).T_{background} - (1-\varepsilon_{sand}).T_{background})$$

with ε_{mine} and ε_{sand} the emissivity of the mine and sand respectively, $T_{mine,cont}$ and $T_{sand,\ cont}$ the contact temperatures of the mine and sand respectively and $T_{mine,app}$ and $T_{sand,app}$ the apparent temperatures of the mine and sand respectively.
Although the apparent and contact temperature of the mines and sand are known, the emissivity of the sand and mines could not be estimated because:

1. $T_{background}$ depends on sky irradiance, cloud cover, ambient temperature and sand temperature. This dependency however is unknown for the time being.
2. $T_{background}$ is different for the top of a mine, the side of a mine and the sand because the observed background area is different.
3. $T_{sand,app}$ is different for several positions in the minefield, probably due to the differences in moisture.
4. Visual inspection of the mine surface gave the impression that the emissivity of the mine ε_{mine} and sand ε_{sand} are not constant over the surface of the mine or sand.

5. CONCLUSIONS

The main conclusions based on the analysis so far, are:

1. With the high resolution DUDA scanner operating in 8-13.4 μm all the surface laid mines are detectable against a sand back ground during a complete diurnal cycle, except for a small period. This holds for metal and plastic AT and AP mines.
2. With the DUDA system the targets could not be detected for only several minutes during a day. This holds for metal and plastic AT and AP mines.
3. Several of the buried mines were detectable during two periods of the day, namely around sunrise and sunset. The mines were detected with the DUDA system
4. The average apparent contrast between the mines and the sand varies from -5 °C to +5 °C.
5. The apparent temperature contrast between the top and the side of a mine is often as big as the apparent temperature contrast between the mine and the sand. Therefore not only average apparent temperature contrasts should be used as criteria for the detection of mines[5].
6. The emissivity of mines and sand could not be determined, although the contact and apparent temperatures of the mine and sand are known.

Overall conclusion: in sand surface laid metal and plastic AP and AT mines can be detected during the whole day with a high resolution TIR scanner operating in 8-13.4 μm. Under these circumstances surface laid mines can be detected during sunset and sunrise.

6. FUTURE ACTIVITIES

- Evaluation of the data recorded with the VIS, NIR and other TIR sensors.
- Evaluate data against mine detection algorithms.
- Compare data with data of other sensors.
- Evaluate data with models that predict TIR and VIS contrast of mines.

7. ACKNOWLEDGEMENTS

We thank the DMKL GEVST-MUN group of the Dutch MOD, UK DRA and the EO and TD group of TNO-FEL for their support before and during the experiment. The discussions with and work of the Remote Sensing and Electro Optics group of TNO-FEL were of help for the data analysis. The work was performed under contract for the Royal Netherlands Army.

8. REFERENCES

[1] "Evaluation of Thermal Viewers for Mine Detection", H. Keller, E. Nawrocki, P. Ngan and A. Trang, report Number 2526, US Army Belvoir RD&E Center, May 1992

[2] "A Characterisation of Diurnal and Environmental Effects on Mines and the Factors Influencing the Performance of Mine Detection ATR Algorithms", G. Maksymonko, B. Ware and D. Poole, In Proc. SPIE Aerosence, "Detection Technologies for Mines and Minelike Targets", April 1995, pp. 140-151.

[3] "Remote Land Mine(Field) detection, an overview of techniques", J.S. Groot and Y.H.L. Janssen, FEL-94-A205, TNO-FEL, The Hague, The Netherlands, 1994

[4] "Multi-sensor fusion for the detection of mines and "mine like" targets", T. Hansow, In Proc. SPIE Aerosence, "Detection Technologies for Mines and Minelike Targets", April 1995, pp. 152-158.

[5] "Detecting Buried Objects by Fusing Dual-Band Infrared Images", G.A. Clark, S.K. Sengupta, M.R. Buhl, R.J. Sherwood, P.C. Schaich, N.Bull et al., Conference record of the twenty-seventh Asilomar Conference, 1993, vol. 1, p 135-143

[6] "Dual Band Capabilities for Imaging Buried Object Sites", N.K. Del Grande, P.F. Durbin, M.R. Gorvad, D.E. Perkins et al., In Proc. SPIE Aerosence, "Underground and Obscured Object Imaging and Detection", April 1993, pp. 166-177.

[7] "Dual-Band Infrared Imaging Applications: Locating Buried Minefields, Mapping Sea Ice, And Inspecting Aging Aircraft", N.K. Del Grande. P.F. Durbin and D.E. Perkins, In Proc. Quantitative Nondestructive Evaluation Conference, San Diego, Ca, July 1992

[8] "Landmine detection with an imaging 94 GHz radiometer", J. Groot, R. Dekker and L. van Ewijk, In Proc. SPIE Aerosence, "Detection Technologies for Mines and Minelike Targets", 1996

[9] "Operating manual of the DUDA II Calibrated Thermal Imaging System", A.N. de Jong, R. Kemp, J. Winkel, M. Roos and W. van Bommel, internal TNO-FEL report, to be published, 1995

[10] "MRTD metingen aan warmtebeeld camera's", S.J.M. Bakker and M.J.J. Roos, FEL 1989-118, TNO-FEL, The Hague, The Netherlands, 1989

[11] "The Infrared & Electro-Optical Handbook", G.J. Zissis et al., SPIE Optical engineering Press, 1993

PROCEEDINGS
SPIE—The International Society for Optical Engineering

Detection and Remediation Technologies for Mines and Minelike Targets

Abinash C. Dubey
Robert L. Barnard
Colin J. Lowe
John E. McFee
Chairs/Editors

9–12 April 1996
Orlando, Florida

Sponsored and Published by
SPIE—The International Society for Optical Engineering

Cooperating Organization
IEE–The Institution of Electrical Engineers

Volume 2765

SPIE is an international technical society dedicated to advancing engineering and scientific applications of optical, photonic, imaging, electronic, and optoelectronic technologies.